Dalton Transactions

ROYAL SOCIETY OF CHEMISTRY

PAPER

View Article Online
View Journal | View Issue

Cite this: *Dalton Trans.*, 2025, **54**, 17180

Tetra- and penta-coordinated aluminum complexes with bis-amidine ligands and their reactivity for efficient CO_2 transformation to cyclic carbonates

Alejandra Acuña,[a,b] Nery Villegas-Escobar,[c] Fernando Gómez Zamorano,[a,b] Nicole Keim-Gyllen,[b] Sonia Mallet-Ladeira,[d] Eddy Maerten,[a] David Madec *[a] and René S. Rojas *[b]

The development of efficient catalysts for CO_2 transformation into value-added products is crucial for sustainable chemistry. In this work, we report the synthesis and characterization of a new series of tetra- and penta-coordinated aluminum complexes supported by bis-amidine ligands featuring a rigid naphthalene bridge and their application as catalysts in the reaction of carbon dioxide with epoxides to form cyclic carbonates. Interestingly, while tetra- and penta-coordinated aluminum complexes bearing methyl groups are efficient when used with TBAI as a co-catalyst, their iodo analogs proved to be inefficient in mono-component catalysis, requiring the use of additional TBAI. Computational results of the proposed systems reveal the necessity of achieving a delicate balance between the nucleophilic properties of iodide atoms and the steric configuration of the complexes. Experimental and computational studies offer valuable insights into the role of ligand structure in aluminum-based catalysts, highlighting the potential of main-group metals in CO_2 fixation.

Received 16th September 2025,
Accepted 17th October 2025

DOI: 10.1039/d5dt02221e

rsc.li/dalton

Introduction

Research in the field of coordination chemistry has contributed enormously to the current development of transition metal chemistry, which plays a crucial role in homogeneous catalysis. Indeed, the properties of transition metal catalysts can be carefully tuned through ligand design and metal selection, making them applicable in a wide variety of fields. Thus, transition metal complexes can act as catalysts to accelerate reactions, activate substrates, and/or reduce the energy costs of many industrial processes (olefin metathesis, hydroformylation, polymerization processes, *etc.*) and as catalysts to directly convert CO_2 into high value-added chemicals.[1–3] Utilizing CO_2 as a raw material for organic compound production adds value and could help offset the costs of its capture and storage. Additionally, it offers an alternative to reduce dependence on fossil fuels for chemical production.[4,5] In this context, the formation of cyclic carbonates from epoxides and carbon dioxide has emerged as one of the most extensively studied methods for carbon dioxide fixation in recent years. On the other hand, cyclic carbonates are valuable as solvents for electrolytes in lithium-ion batteries, as polar aprotic solvents, and as intermediates in the synthesis of different small molecules and polymers.[6,7] These cyclic carbonates can be synthesized through reactions between epoxides and CO_2, using several organometallic complexes as catalysts (Scheme 1). In these catalytic processes, systems combining Lewis acids and nucleophiles are required. The metal center serves as the Lewis acid, activating the epoxide, while a cocatalyst provides a halide that acts as a nucleophile, inducing ring-opening.[8]

[a]*Laboratoire Hétérochimie Fondamentale et Appliquée, Université de Toulouse, Centre National de la Recherche Scientifique (CNRS), UMR 5069, 118 Route de Narbonne, 31062 Toulouse Cedex 09, France. E-mail: david.madec@univ-tlse3.fr*
[b]*Departamento de Química Inorgánica, Facultad de Química y de Farmacia, Pontificia Universidad Católica de Chile, Vicuña Mackenna 4860, 7820436 Macul, Santiago, Chile. E-mail: rrojasg@uc.cl*
[c]*Departamento de Físico-Química, Facultad de Ciencias Químicas, Universidad de Concepción, Concepción 4070139, Chile*
[d]*Institut de Chimie de Toulouse (UAR 2599), 118 Route de Narbonne, 31062 Toulouse Cedex 09, France*

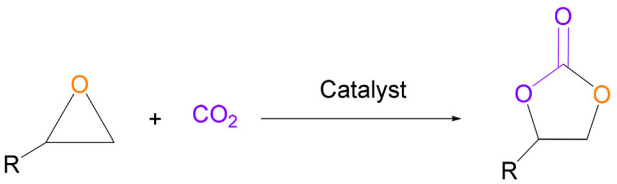

Scheme 1 Synthesis of cyclic carbonates from epoxides and CO_2.

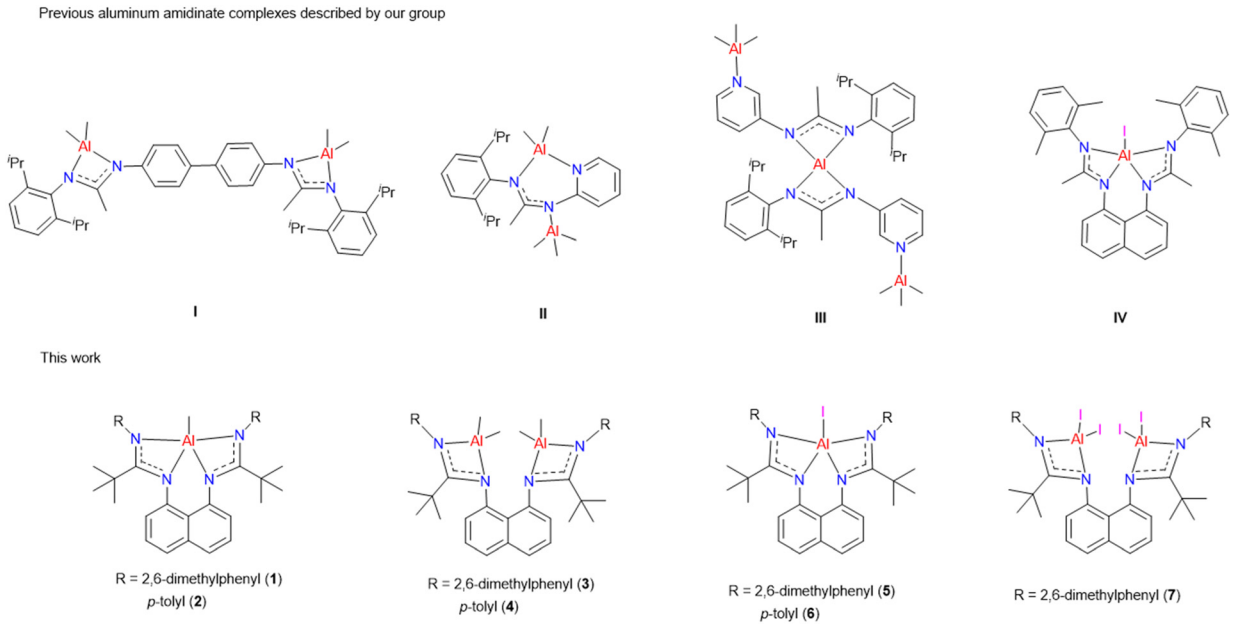

Fig. 1 Double aluminum amidinate, bi- and tri-aluminum amidinate and pentacoordinate bis-amidinate complexes described by our group.

As an alternative to transition metals, nowadays the chemistry of main-group element complexes, capable of mimicking transition metal behavior, is experiencing significant development. In particular, recent research has demonstrated that aluminum derivatives, the third most abundant element in the Earth's crust with low toxicity and low production costs, behave quite similarly to transition metal complexes and are able to activate strong bonds in small molecules (H_2, N_2, CO, and CO_2).[9,10]

Since the choice of ligands is essential in each organometallic process, amidinate ligands, which are endlessly versatile in their potential structure and substitution patterns, have attracted attention for the stabilization of aluminum species.[11] Indeed, they present high basicity with a pK_a value of approximately 12 and therefore exhibit good affinity for protons and Lewis acids.[12,13] Amidinate aluminum complexes have shown promising catalytic activity in various processes, such as ring-opening polymerization, alkyne hydroboration and the conversion of CO_2 to cyclic carbonates.[11k,l,n]

In recent years, our research group has reported a series of aluminum amidinate complexes as catalysts for synthesizing cyclic carbonates from CO_2 and epoxides.[14–16] The first symmetric aluminum bimetallic complex **I** (a double aluminum amidinate, see Fig. 1) proved to be an excellent catalyst (conversions between 62 and 100% in 24 h) in the presence of tetrabutylammonium iodide (TBAI) as a co-catalyst.[14] Bi- and tri-metallic aluminum-amidinate complexes were also reported (Fig. 1, **II** and **III**, respectively) as efficient catalysts for the formation of cyclic carbonates from terminal epoxides and CO_2 at 50 °C under 1 bar of CO_2 pressure without solvent.[15] In 2021, a pentacoordinate bisamidinate iodide aluminum complex **IV** (Fig. 1) was reported, which is one of the first examples of a neutral non-zwitterionic aluminum complex used as a single-component catalyst for the synthesis of carbonates (catalytic activity at 80 °C and 1 bar of CO_2, without a co-catalyst).[16]

As part of our ongoing interest in designing new aluminum complexes for catalytic applications, this work reports the synthesis and structural characterization of a new series of tetra- and penta-coordinated aluminum complexes with amidinate ligands featuring a rigid naphthalene bridge (**1**–**7**, Fig. 1). The performance and reactivity of these complexes were evaluated as catalysts in the reaction of carbon dioxide with epoxides to form cyclic carbonates. The influence of the substitution pattern on the amidinate ligand was explored to understand how these variations affect the catalytic activity and selectivity of the corresponding aluminum complexes.

Results and discussion

Synthesis of aluminum complexes

Aluminum complexes **1**–**4** were synthesized through protonolysis reactions between the corresponding bis(amidine) ligands ($\mathbf{L_1H_2}$ or $\mathbf{L_2H_2}$) and one or two equivalents of $Al(CH_3)_3$ (Scheme 2). These reactions were easily monitored by gas bubble evolution (CH_4). Complex **1** was obtained through the reaction of one equivalent of $\mathbf{L_1H_2}$ and one equivalent of $Al(CH_3)_3$ in dry benzene at 60 °C for 2 hours because of the high steric hindrance. Complex **1** was isolated as a yellow solid in 93% yield. The formation of a pentacoordinate aluminum complex was established by NMR spectroscopy. The ^{1}H NMR spectrum showed the disappearance of the resonance corresponding to the N–H groups of ligand $\mathbf{L_1H_2}$. Additionally, the methyl group coordinated to the aluminum atom is easily identified in ^{1}H and ^{13}C NMR spectra, each exhibiting a

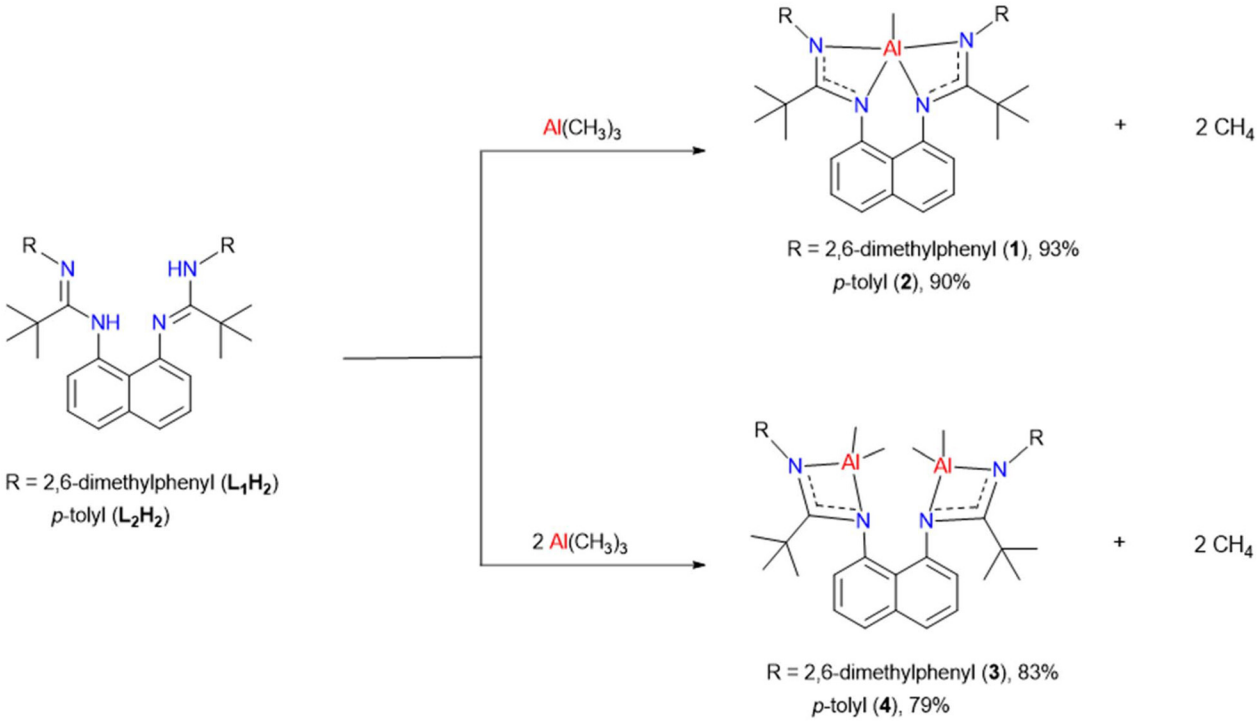

Scheme 2 Synthesis of penta-coordinated aluminum (**1** and **2**) and tetra-coordinated bis-aluminum (**3** and **4**) complexes.

characteristic signal in the negative region, respectively, at −0.34 ppm and −4.28 ppm, in good agreement with previously reported pentacoordinate aluminum complexes.[16] The ^{1}H and ^{13}C NMR resonance patterns support the existence of a plane of symmetry in this complex. On the other hand, $\mathbf{L_2H_2}$ reacts much faster and smoothly with one equivalent of $Al(CH_3)_3$ in CH_2Cl_2 at room temperature, affording the pentacoordinate aluminum complex **2** as a yellow solid in 90% yield within only one hour. Similarly, the methyl group coordinated to the central aluminum atom appears at −0.89 ppm and −3.99 ppm in the respective ^{1}H and ^{13}C NMR spectra.

The bis-aluminum complex **3** was synthesized using 1 equivalent of $\mathbf{L_1H_2}$ and two equivalents of $Al(CH_3)_3$ in dry toluene at room temperature for 1 hour. Complex **3** was obtained as orange crystals in 83% yield. The formation of the corresponding bis-aluminum complexes was established by NMR spectroscopy and corroborated by XRD analysis (Fig. 2). The ^{1}H NMR spectrum exhibited two signals in the negative region at −0.02 and −0.33 ppm, each integrating for 6 H, indicating that each aluminum atom is tetracoordinated with one amidinate ligand and two CH_3 groups in its structure. In the ^{13}C NMR spectrum, the signals of the methyl groups coordinated to the aluminum atoms appeared at −5.41 and −9.16 ppm.

Finally, the analogous aluminum complex **4** was obtained when $\mathbf{L_2H_2}$ is mixed with two equivalents of $Al(CH_3)_3$. The NMR data are very similar to those of complex **3** with signals at −0.33 and −0.75 ppm that integrate for 6 H in the ^{1}H NMR spectrum.

To gain more insight into these electronic structures, quantum chemical calculations were performed. Each molecular structure was optimized by employing density functional theory (DFT) calculations at the ωB97XD/def2-TZVP level of theory. Geometric indexes, such as τ_5 and τ_4, were computed at the DFT level. Molecular electrostatic potentials (MEPs) were calculated for all systems and are shown in Fig. 3. At first glance, this analysis underscores notable variations in electronic distribution that can be attributed to the effects of substitution either at the aluminum center or at the ligand.

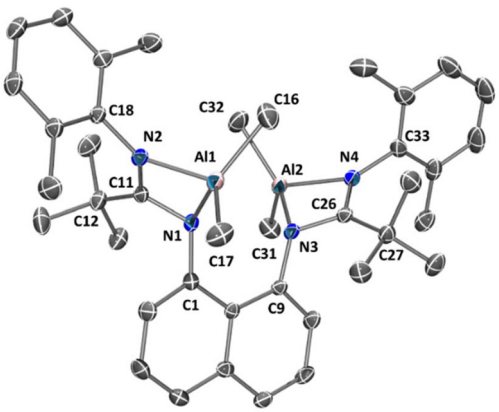

Fig. 2 Molecular structure of **3** (hydrogens are omitted for clarity). Thermal ellipsoids are shown at 50% probability. Selected bond lengths (Å) and angles [°]: C16–Al1 1.948(4), C17–Al1 1.956(4), Al1–N2 1.942(3), Al1–N1 1.948(3), Al2–N3 1.942(3), Al2–N4 1.954(3), C11–N2 1.333(4), C11–N1 1.375(4), C26–N4 1.335(4), C26–N3 1.369(4), C31–Al2 1.954(4), C32–Al2 1.949(4); N2–C11–N1 108.5(3), N4–C26–N3 108.7(3).

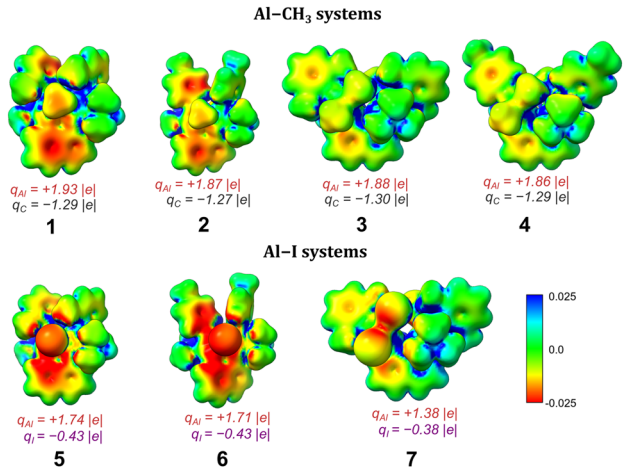

Fig. 3 Molecular electrostatic potential (MEP) for all complexes (isosurface 0.01 au). NPA charges (q_i) for selected atoms are displayed.

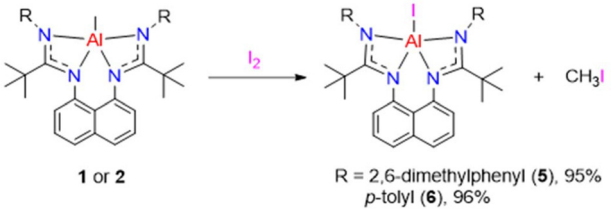

Scheme 3 Synthesis of complexes **5** and **6**.

The DFT-optimized molecular structures of complexes **1** and **2** confirmed a pentacoordinate Al center with τ_5 indexes[17] of 0.35 and 0.28, suggesting a distorted square pyramidal geometry at the Al centers. The computed equilibrium Al–C distances (bond orders) were 1.967 Å (0.56) and 1.965 Å (0.58), for complexes **1** and **2**, respectively. Fig. 3 reveals that the Al atom in complex **1** exhibits a depletion of the electron density shown as a more positive atomic charge, while the C atom exhibits a more pronounced negative charge compared to complex **2**. This observation is further supported by the comparative analysis of bond distances, bond orders, and atomic charges. Specifically, the longer bond distance and lower bond order, coupled with the greater charge separation of the Al–C bond in complex **1**, unequivocally indicate a more polar Al–C covalent bond in this system compared to complex **2**. Besides the small differences observed, these indexes still highlight the effect of the different R groups in both ligands. The τ_4 index[18] computed from the XRD and DFT structures was 0.95 and 0.94, which supports the use of the DFT structures for structural comparison. However, for a fair comparison, only the DFT-derived indexes are discussed. The τ_4 indexes computed from the DFT structures were found to be 0.95 and 0.96 for complexes **3** and **4**, respectively, confirming the distorted tetrahedral structure at Al. Interestingly, the DFT structures of the aluminum complexes reported slightly different Al–C bond distances for each Al center in complex **3** of 1.963 Å and 1.957 Å, respectively. However, the respective bond order remains similar for both distances around 0.67. The indistinguishable bond distances of N–C in the NCN unit and almost equal N–Al bond distances proved the formation of a delocalized system.

In a previously reported article, we have established that THE incorporation of a nucleophile (iodide) at the aluminum center could be an interesting strategy to obtain a single-component catalyst (avoiding the use of ammonium iodide as a cocatalyst). Indeed, the reaction mechanism has been shown to require an epoxide–iodide exchange at the aluminum atom, with an activation free energy of ~20 kcal mol^{-1} for styrene oxide.[16]

For the pentacoordinate aluminum complexes, the formation of the respective iodide derivatives was achieved by reacting the corresponding complex (**1** or **2**) with one equivalent of I_2 using a method previously described (Scheme 3).

Compounds **5** and **6** were obtained as brown solids in 95% and 96% yields, respectively. The products were fully characterized by NMR spectroscopy. These reactions were easily monitored by ^{1}H NMR, with the disappearance of the signal corresponding to the methyl group at the aluminum center.

The NMR patterns of both iodo-complexes **5** and **6** again indicate molecular symmetry.

The optimized DFT structures of iodine-containing complexes (complexes **5** and **6**) show Al–I bond distances of 2.565 Å (a bond order of 0.82) for complex **5** and a slightly shorter bond length of 2.547 Å (a bond order of 0.85) for complex **6**. Notably, the NBO charges at the iodine centers remain consistent, with only minor variations in the electron population at the aluminum center. This significant electron density difference between Al and I suggests a polarized covalent bond, an essential characteristic for their function as single-component catalysts (*vide infra*). The MEP of complexes **5** and **6** (Fig. 3) indicates charge accumulation on the iodine atom, with delocalization across the ligand backbone. This delocalization is more pronounced in complex **6**, extending between the naphthalene and phenyl groups due to the complex's relatively planar conformation.

In the case of the bis-aluminum complexes **3** and **4**, attempts to replace the methyl groups with iodide using I_2 with the present procedure were unsuccessful in our hands, resulting in mixtures of products that were difficult to identify. As an alternative synthetic route, BI_3 was used as a source of iodides to carry out the substitution. The reaction between **3** and 2 equivalents of BI_3 was carried out in benzene at room temperature for 1 hour (Scheme 4), resulting in the isolation of compound **7** as yellow crystals (91% yield). As before, the evident disappearance of signals in the negative region of the ^{1}H NMR spectrum was a good indicator of reaction completion. Complex **7** presents an extremely low solubility in common solvents, preventing us from acquiring the corresponding ^{13}C NMR spectrum. However, the formation of the bis-(iodo)complex was established by DRX analysis (Fig. 4), which revealed that the aluminum atoms exhibit a distorted tetrahedral geometry.

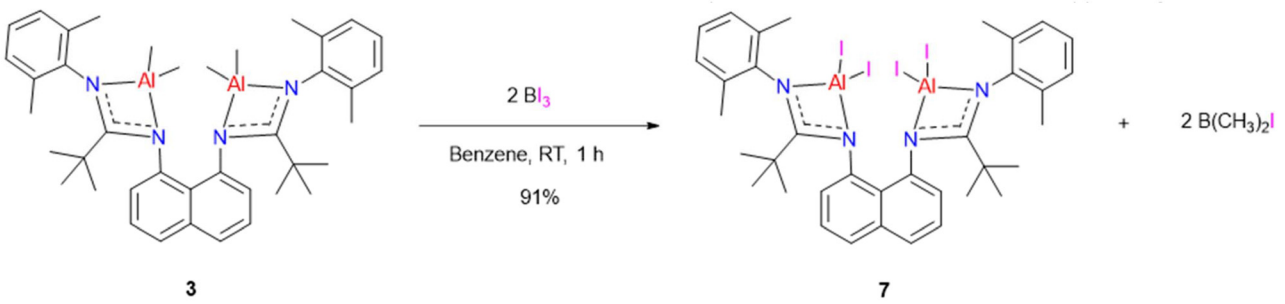

Scheme 4 Synthesis of **7**.

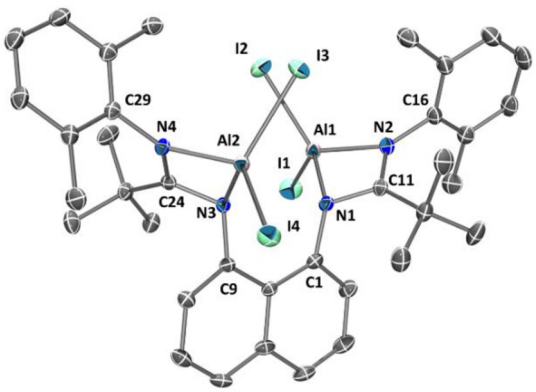

Fig. 4 Molecular structure of **7** (hydrogens are omitted for clarity). Thermal ellipsoids are shown at 50% probability. Selected bond lengths (Å) and angles [°]: Al1–N1 1.894(2), Al1–N2 1.906(2), Al1–I2 2.4847(9), Al1–I1 2.4949(9), C11–N2 1.331(3), C11–N1 1.371(3), Al2–N3 1.901(2), Al2–N4 1.905(2), Al2–I3 2.4987(8), Al2–I4 2.4996(8), C24–N4 1.330(3), C24–N3 1.385(3); N2–C11–N1 108.8(2), N4–C24–N3 108.8(2).

For the bimetallic complex **7**, the MEP surface reveals a distinctive electronic distribution influenced by the presence of two Al–I bonds. By comparing the atomic charges at the Al and I centers, we gain insights into the polarity of these bonds.[19] The results show that the Al–I bonds in complex **7** are approximately 20% less polar than those in complexes **5** and **6**. Consequently, this reduced polarity of the two covalent bonds in complex **7** may suggest lower reactivity, limiting its efficacy as a single-component catalyst for cyclic carbonate formation.

Surprisingly, the replacement of methyl groups in complex **4** with iodides to form the halogenated complex led to a thermally unstable species. Indeed, at low temperature (−78 °C), the ^{1}H spectrum indicates that the reaction proceeds similarly to the previously reported complexes **1–3**. Above this temperature, decomposition occurred, making it impossible to isolate the iodocomplex.

Catalytic study for the synthesis of cyclic carbonates

With complexes **1–7** in hand, we explored their use as catalysts for the preparation of a range of cyclic carbonates (**9a–h**) from their corresponding epoxides (**8a–h**) and CO_2 under solvent-free conditions. The results of the catalytic runs are shown in Fig. 5. The reactions were carried out at 80 °C under 1 bar of CO_2 pressure for 24 h employing a combination of 1.5 mol% of complexes **1** or **2** and 1.5 mol% of TBAI as a cocatalyst and 0.75 mol% of complexes **3** or **4** with 1.5 mol% of TBAI for dual component systems. For one-component systems, only 1.5 or 0.75 mol% of catalysts **5**, **6** or **7** were used. As expected, under these reaction conditions, no polycarbonates were obtained. Catalysts **1–4** associated with TBAI achieved moderate to excellent yields (50–97%) for the preparation of cyclic carbonates **9a–9h** (Fig. 5).[8,11,14–16] No clear trend can be identified regarding the effectiveness of these systems based on the electronic or steric effects triggered by the R substituent in the starting epoxide, demonstrating that these systems exhibit good efficiency and broad scope.

Generally, complexes **3** and **4** exhibited slightly better efficiency than complexes **1** and **2**. For the mono-component catalysts **5**, **6**, and **7**, the results were disappointing. Indeed, no catalytic activity could be detected for catalysts **5** and **7**, and

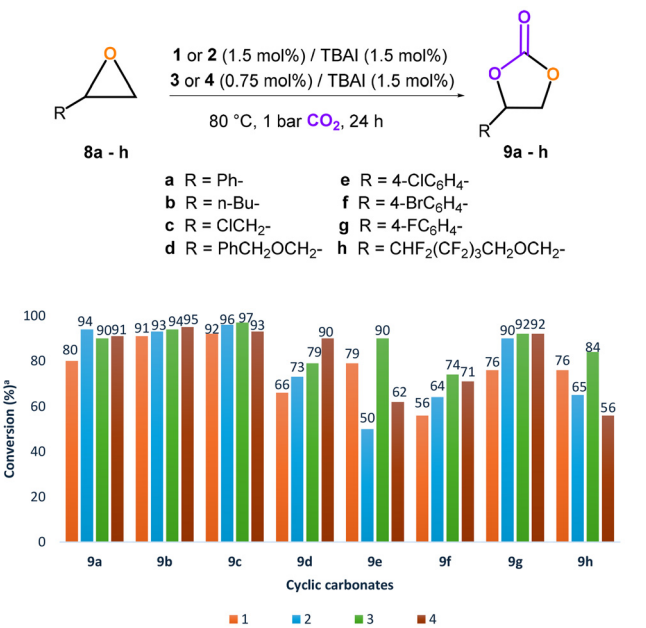

Fig. 5 Conversion of cyclic carbonates **9a–h** employing catalysts **1–7**. [a] Determined by ^{1}H NMR spectroscopy of the crude reaction mixture.

extremely low conversions were observed with catalyst **6** for three substrates (8, 3 and 9% conversion for substrates **9a**, **9e**, **9g**, respectively). Specifically, the absence or the poor catalytic activity of compounds **5**, **6** and **7** can be attributed to the poor polarity of the Al–I bonds as shown by the MEP surface (Fig. 3) that probably prevents (or limits) the liberation of the iodide atom. The X-ray data obtained in the case of complex **7** corroborate this hypothesis, with Al–I bond lengths rather short (between 2.4847 and 2.4996 Å) when compared to the one observed in a similar active one-component system (2.553 Å) with a similar ligand reported by our research group.[16]

To further understand the absence of reactivity of **5** and the limited reactivity of **6**, we examined the geometries of these complexes by DFT when functioning as single-component catalysts. A critical comparison with the reactive system **IV** (Fig. 1) suggests that the pivotal step in these new complexes is the initial stage of the mechanism, involving the epoxide–iodide exchange at the aluminum center. The transition-state structure ($\mathbf{TS_{IV+a}}$) of complex **IV** during this exchange with styrene oxide (**a**) is depicted in Fig. 6. Concurrently, steric maps illustrating the computed free volume in the frontal regions of systems **5** and **6** are also presented in Fig. 6.

It is important to note that complexes **IV** and **5** differ only in the R substituent linked to the amidine moiety, with methyl in **IV** and ^{t}butyl in complex **6**. Although this substitution might seem minor, the bulkier ^{t}butyl substituent in complex **5** significantly hampers its reactivity as a single-component catalyst. The steric maps in Fig. 7 further detail the approximate entry channel for the epoxide and the exit channel for the iodide atom, consistent with the transition state structure shown on the left. As illustrated, the ^{t}butyl group on the amidine moiety, along with the methyl groups on the phenyl rings, obstructs both the entry channel for the epoxide and the exit channel for the iodide, thereby inhibiting the reaction mechanism.

Conversely, the low reactivity of complex **6** towards the selected epoxide can be attributed to more open entry and exit channels, coupled with a larger free volume. This is achieved by retaining the bulky ^{t}butyl groups while positioning the methyl group on the phenyl rings at the *para* position. Computational analysis of the systems suggests that achieving an optimal balance between the nucleophilic nature of the iodide atoms and the steric demands of the complexes, which facilitates favorable entry and exit channels for the exchange of epoxide and iodide atoms, is crucial for the future design of single-component catalysts.

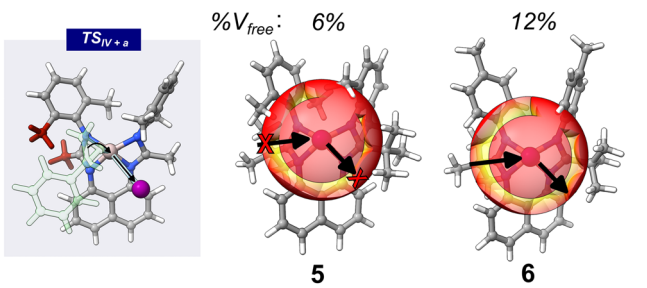

Fig. 6 Illustration of the transition state structure for the reaction between complex **IV** and styrene oxide (**a**). Key methyl groups in the ligand are highlighted in red, while the epoxide is rendered transparent for enhanced clarity (inset box). Steric maps of complexes **5** and **6** are presented, showing the computed free volume percentage in the frontal region of the complexes. Arrows indicate the entry pathway of the epoxide and the exit route of iodide atoms.

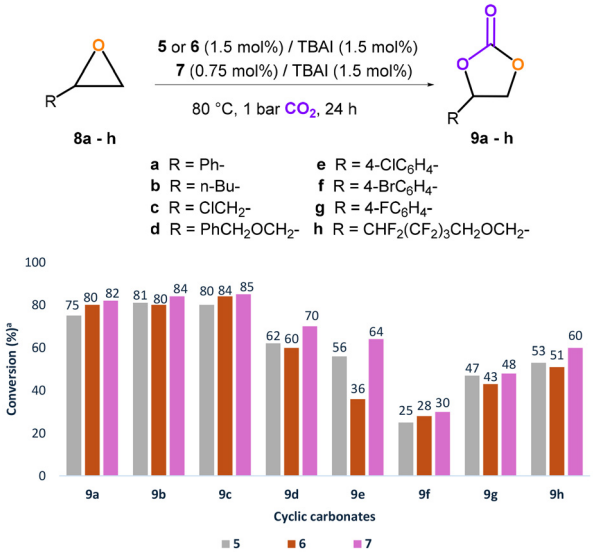

Fig. 7 Conversion of cyclic carbonates **9a–h** employing catalysts **5**, **6**, and **7**. [a] Determined by ^{1}H NMR spectroscopy of the crude reaction mixture.

To investigate whether the lack of catalytic activity of complexes **5**, **6**, and **7** as one-component systems is due to the non-dissociation of the iodide ligand, we employed these complexes in the presence of TBAI as a cocatalyst, keeping all the other experimental conditions unchanged.

The conversions are depicted in Fig. 7, demonstrating that the simple addition of TBAI as a cocatalyst leads to an active system for every studied substrate. The efficiency of the mono- and bimetallic catalysts is very similar for every substrate. It is worth noting that the catalytic activity of iodoaluminum complexes is slightly lower than that of their methylated analogs.

These new catalytic systems show interesting reactivities, comparable to those previously described in the literature.[11k–n,14–16] The recyclability of the catalyst, due to the type of catalysis (homogeneous catalysis) and the experimental conditions (without solvent, mol%...), is not possible.

Conclusions

In this study, we synthesized and characterized a series of tetra- and penta-coordinated aluminum complexes with bis-amidine ligands and evaluated their catalytic performance in the conversion of CO_2 and epoxides into cyclic carbonates. The results highlight the significant influence of ligand structure

on the catalytic efficiency and selectivity of these aluminum complexes. While tetra- and penta-coordinated aluminum complexes **1–4** bearing methyl groups are efficient when used with TBAI as a co-catalyst, their iodo analogs **5–7** proved to be inefficient in mono-component catalysis, requiring the use of additional TBAI. Computational results of the proposed systems reveal the necessity of achieving a delicate balance between the nucleophilic properties of iodide atoms and the steric configuration of the complexes, which is pivotal for facilitating effective entry and exit channels in the design of future single-component catalysts. This study underscores the potential of aluminum-based catalysts as sustainable alternatives for CO_2 fixation. Future research should focus on further ligand modifications (electronic and steric) to enhance the catalyst reactivity and obtain efficient single-component catalysts for cyclic carbonate synthesis.

Experimental

General information

All manipulations were performed under an inert atmosphere of argon or nitrogen using standard Schlenk line and glovebox techniques. Dry, oxygen-free solvents were employed. Reagents were obtained from commercial suppliers unless otherwise stated. *N*,*N*′-(naphthalene-1,8-diyl)bis(2,2-dimethylpropanamide),[20] *N*,*N*′(naphthalene-1,8-diyl)bis(2,2-dimethylpropanimidoyl chloride),[20] L_1H_2,[21] and L_2H_2 [21] were synthesized following reported procedures. 1D and 2D NMR spectra were recorded with the following spectrometers for ^1H and ^{13}C: Bruker Avance II 300 MHz, Avance III HD 400 MHz, and Avance I and II 500 MHz spectrometers. The chemical shifts were counted positively relative to the low field and expressed in parts per million (ppm). Mass spectrometric analyses were performed using a Maldi micro MX micro-mass spectrometer with a pyrene matrix (ratio of product/matrix : 1/100). Melting points were measured with a capillary electrothermal Stuart SMP40 apparatus, and samples were prepared in the glovebox before the analysis. Single-crystal X-ray data were collected at low temperature (193(2) K) on a Bruker D8 VENTURE diffractometer equipped with a PHOTON III detector and using MoK_α radiation (λ = 0.71037 Å). Phi and omega scans were performed for data collection, and an empirical absorption correction was applied.[22] The structures were solved by the intrinsic phasing method (ShelXT)[23] and refined by the full-matrix least-squares method on F^2.[24] All non-hydrogen atoms were refined with anisotropic displacement parameters. All hydrogen atoms were refined isotropically at calculated positions using a riding model, except for those of the water molecules in the structure of compound **3**, which were not located in the difference Fourier maps. For **3**, some electron density was difficult to model; therefore, the SQUEEZE tool[25] of PLATON was used to remove the corresponding electron density from the intensity data.

Deposition numbers 2477633 (**3**) and 2477634 (**7**) contain the supplementary crystallographic data for this paper.

Complexes **1–7** were fully optimized at the ωB97XD/def2-TZVP level of theory, with the resulting structures confirmed by frequency calculations at the same level. Population and bond order analyses were conducted using the NBO3.1 program, interfaced with Gaussian16 Rev B.01. Bond orders were specifically calculated using the Mayer definition, recommended as a suitable method for characterizing bonds in metal complexes due to its incorporation of the overlap matrix in the bond order determination.[26] Molecular electrostatic potentials were computed for all systems at the same level of theory.

Synthesis of complex 1. $Al(CH_3)_3$ (8.12 mg, 0.11 mmol) was added to a solution of $\mathbf{L_1H_2}$ (60 mg, 0.11 mmol) in dry benzene. The mixture was stirred for 2 h at 60 °C. After the solvent was removed, the solid residue was washed with pentane. A yellow solid was obtained (59.5 mg, 0.10 mmol, 93%). **Melting point**: 206 °C. **^{1}H NMR** (C_6D_6, 400 MHz): δ 7.42 (t, J_{HH} = 8.2 Hz, 4H, $C_{10}H_6$), 7.22 (t, J_{HH} = 7.8 Hz, 2H, $C_{10}H_6$), 6.86 (s, 6H, C_6H_3), 2.08 (s, 12H, CH_3), 1.06 (s, 18H, $C(CH_3)_3$), −0.34 (s, 3H, CH_3–Al). **^{13}C{^{1}H} NMR** (C_6D_6, 100 MHz): δ 181.6 (NCN), 144.8 (C_6H_{3ipso}), 142.2 ($C_{10}H_{6ipso}$), 137.4 ($C_{10}H_{6ipso}$), 133.8 (C_6H_{3ipso}), 128.3 (C_6H_3), 126.5 ($C_{10}H_{6ipso}$), 125.2 ($C_{10}H_6$), 124.6 (C_6H_3), 123.4 ($C_{10}H_6$), 121.0 ($C_{10}H_6$), 39.9 ($\underline{C}(CH_3)_3$), 29.5 ($C(\underline{C}H_3)_3$), 19.7 (CH_3), −4.3 (CH_3–Al).

Synthesis of complex 2. $Al(CH_3)_3$ (28.6 mg, 0.39 mmol) was added to a solution of $\mathbf{L_2H_2}$ (200 mg, 0.39 mmol) in dry CH_2Cl_2. The mixture was stirred for 1 h at room temperature. After the solvent was removed, the solid residue was washed with pentane. A yellow solid was obtained (192 mg, 0.35 mmol, 90%). **Melting point**: 238 °C. **^{1}H NMR** ($CDCl_3$, 400 MHz): δ 7.42 (d, J_{HH} = 8.2 Hz, 2H, $C_{10}H_6$), 7.30–7.24 (m, 2H, $C_{10}H_6$), 7.18 (d, J_{HH} = 7.4 Hz, 2H, $C_{10}H_6$), 7.00 (d, J_{HH} = 7.9 Hz, 4H, C_6H_4), 6.81 (d, J_{HH} = 7.9 Hz, 4H, C_6H_4), 2.31 (s, 6H, CH_3), 1.34 (s, 18H, $C(CH_3)_3$), −0.89 (s, 3H, CH_3–Al). **^{13}C{^{1}H} NMR** ($CDCl_3$, 100 MHz): δ 181.0 (NCN), 143.7 (C_6H_{4ipso}), 142.7 ($C_{10}H_{6ipso}$), 136.8 ($C_{10}H_{6ipso}$), 132.3 (C_6H_{4ipso}), 129.3 (C_6H_4), 125.2 ($C_{10}H_6$), 124.6 (C_6H_4), 123.0 ($C_{10}H_6$), 122.5 ($C_{10}H_{6ipso}$), 120.3 ($C_{10}H_6$), 40.5 ($\underline{C}(CH_3)_3$), 31.1 ($C(\underline{C}H_3)_3$), 21.0 (CH_3), −4.0 (CH_3–Al).

Synthesis of complex 3. A 2 M solution of $Al(CH_3)_3$ in heptane (1.9 mL, 3.8 mmol) was added to a solution of $\mathbf{L_1H_2}$ (1.0 g, 1.9 mmol) in toluene (20 mL) in a Schlenk flask. The mixture was stirred for 2 h at room temperature. After the solvent was removed, the solid residue was washed with pentane (5 × 10 mL). An orange solid was recrystallized from pentane at −30 °C. Orange crystals were obtained (1.07 g, 1.7 mmol, 83%). **Melting point**: 200 °C. **^{1}H NMR** (C_6D_6, 500 MHz): δ 7.44 (dd, J_{HH} = 8.1, 1.0 Hz, 2H, $C_{10}H_6$), 7.18–7.16 (overlapped, 2H, $C_{10}H_6$), 7.11–7.07 (m, 2H, $C_{10}H_6$), 7.00–6.91 (m, 6H, C_6H_3), 2.55 (s, 6H, CH_3), 2.52 (s, 6H, CH_3), 0.95 (s, 9H, $C(CH_3)_3$), −0.02 (s, 6H, CH_3–Al), −0.33 (s, 6H, CH_3–Al). **^{13}C{^{1}H} NMR** (C_6D_6, 125 MHz): δ 186.9 (NCN), 144.6 ($C_{10}H_{6ipso}$), 142.4 (C_6H_{3ipso}), 137.9 ($C_{10}H_{6ipso}$), 133.9 (C_6H_{3ipso}), 132.8 (C_6H_{3ipso}), 129.0 (C_6H_3), 128.7 (C_6H_3), 127.1 ($C_{10}H_{6ipso}$), 126.6 ($C_{10}H_6$), 126.6 ($C_{10}H_6$), 125.7 ($C_{10}H_6$), 125.1 ($C_{10}H_6$), 41.3 ($\underline{C}(CH_3)_3$), 29.8 ($C(\underline{C}H_3)_3$), 20.7 (CH_3), 20.5 (CH_3), −5.4 (CH_3–Al), −9.2

(CH_3–Al). **MS** (Maldi-TOF) *m*/*z*: 643.21 ($[M]^+$), 629.17 ($[M - CH_3]^+$), 615.16 ($[M - 2(CH_3)]^+$).

Synthesis of complex 4. A 2 M solution of $Al(CH_3)_3$ in heptane (0.6 mL, 1.2 mmol) was added to a solution of $\mathbf{L_3H}$ (300 mg, 0.60 mmol) in toluene (6 mL) in a Schlenk flask. The mixture was stirred for 2 h at room temperature. After the solvent was removed, the solid residue was washed with pentane (5 × 10 mL). A yellow solid was obtained (295.0 mg, 0.48 mmol, 79%). **Melting point**: 221 °C. **^{1}H NMR** ($CDCl_3$, 300 MHz): δ 7.63 (d, J_{HH} = 8.2 Hz, 2H, $C_{10}H_6$), 7.32 (t, J_{HH} = 7.7 Hz, 2H, $C_{10}H_6$), 7.16 (s, 8H, C_6H_4), 6.99 (d, J_{HH} = 7.3 Hz, 2H, $C_{10}H_6$), 2.36 (s, 6H, CH_3), 0.89 (s, 18H, $C(CH_3)_3$), −0.33 (s, 6H, CH_3–Al), −0.75 (s, 6H, CH_3–Al). **^{13}C{^{1}H} NMR** (C_6D_6, 125 MHz): δ 183.9 (NCN), 143.7 ($C_{10}H_{6ipso}$), 142.7 (C_6H_{4ipso}), 137.1 ($C_{10}H_{6ipso}$), 134.7 (C_6H_{4ipso}), 129.9 (C_6H_4), 126.4 ($C_{10}H_6$), 126.1 ($C_{10}H_6$), 125.2 ($C_{10}H_6$), 41.2 ($\underline{C}(CH_3)_3$), 31.0 ($C(\underline{C}H_3)_3$), 20.9 (CH_3), −7.9 (CH_3–Al), −11.0 (CH_3–Al).

Synthesis of complex 5. Benzene was added to **1** (200.0 mg, 0.35 mmol) and I_2 (88.7 mg, 0.35 mmol) in a Schlenk flask. The mixture was stirred for 1 h at room temperature. After the solvent was removed, the solid residue was washed with pentane (3 × 5 mL). A brown solid was obtained (228.0 mg, 0.33 mmol, 95%). **Melting point**: 196 °C (decomposition). **^{1}H NMR** (C_6D_6, 400 MHz): δ 7.54 (dd, J_{HH} = 21.5, 7.8 Hz, 4H, $C_{10}H_6$), 7.33–7.26 (m, 2H, $C_{10}H_6$), 7.04–6.94 (m, 6H, C_6H_3), 2.30 (s, 12H, CH_3), 1.09 (s, 18H, $C(CH_3)_3$). **^{13}C{^{1}H} NMR** (C_6D_6, 100 MHz): δ 183.3 (NCN), 142.9 (C_6H_{3ipso}), 140.4 ($C_{10}H_{6ipso}$), 137.0 ($C_{10}H_{6ipso}$), 134.3 (C_6H_{3ipso}), 128.4 (C_6H_3), 126.5 ($C_{10}H_{6ipso}$), 125.5 (C_6H_3), 125.3 ($C_{10}H_6$), 124.3 ($C_{10}H_6$), 121.8 ($C_{10}H_6$), 39.8 ($\underline{C}(CH_3)_3$), 29.2 ($C(\underline{C}H_3)_3$), 20.4 (CH_3).

Synthesis of complex 6. CH_2Cl_2 was added to **2** (200.0 mg, 0.37 mmol) and I_2 (93.3 mg, 0.37 mmol) in a Schlenk flask. The mixture was stirred for 1 h at room temperature. After the solvent was removed, the solid residue was washed with pentane (3 × 5 mL). A brown solid was obtained (234.0 mg, 0.36 mmol, 96%). **Melting point**: 207 °C. **^{1}H NMR** ($CDCl_3$, 400 MHz): δ 7.47 (dd, J_{HH} = 7.2, 1.7 Hz, 2H, $C_{10}H_6$), 7.33–7.24 (m, 4H, $C_{10}H_6$), 7.01 (d, J_{HH} = 8.0 Hz, 4H, C_6H_4), 6.83 (d, J_{HH} = 8.1 Hz, 4H, C_6H_4), 2.30 (s, 6H, CH_3), 1.35 (s, 18H, $C(CH_3)_3$). **^{13}C{^{1}H} NMR** ($CDCl_3$, 100 MHz): δ 182.3 (NCN), 141.7 (C_6H_{4ipso}), 140.6 ($C_{10}H_{6ipso}$), 136.8 ($C_{10}H_{6ipso}$), 133.7 (C_6H_{4ipso}), 129.5 (C_6H_4), 125.2 (C_6H_4), 125.1 ($C_{10}H_6$), 124.0 ($C_{10}H_6$), 122.2 ($C_{10}H_{6ipso}$), 121.0 ($C_{10}H_6$), 40.6 ($\underline{C}(CH_3)_3$), 30.7 ($C(\underline{C}H_3)_3$), 21.1 (CH_3).

Synthesis of complex 7. Benzene (10 mL) was added to **3** (200.0 mg, 0.31 mmol) and BI_3 (243.0 mg, 0.62 mmol) in a Schlenk flask. The mixture was stirred for 1 h at room temperature, and a white precipitate was observed. After the solvent was removed, the solid residue was washed with pentane (3 × 5 mL). A white solid was recrystallized from benzene at room temperature. Yellow crystals were obtained (307.0 mg, 0.281 mmol, 91%). **Melting point**: 203 °C (decomposition). **^{1}H NMR** (C_6D_6, 300 MHz): δ 7.48–7.39 (m, 4H, $C_{10}H_6$), 7.07–7.02 (m, 2H, $C_{10}H_6$), 6.93–6.83 (m, 6H, C_6H_3), 2.83 (s, 6H, CH_3), 2.70 (s, 6H, CH_3), 0.95 (s, 18H, $C(CH_3)_3$). **MS** (Maldi-TOF) *m*/*z*: 583.3 ($[M - 4I]^+$).

General catalysis protocol. Epoxide (0.2 mL) and the catalysts (**1**–**7**) were placed in glass vials with a magnetic stirring bar in an autoclave reactor. The reaction mixture was stirred at 80 °C under 1 bar of CO_2 pressure for 24 h. For complexes **1** and **2**, the conditions were 1.5 mol% of catalyst and 1.5 mol% of TBAI as a cocatalyst; for complexes **3** and **4**, 0.75 mol% of catalyst and 1.5 mol% of TBAI; for complexes **5** and **6**, 1.5 mol% of catalyst without a cocatalyst; and for complex **7**, 0.75 mol% of catalyst without TBAI. Complexes **5**, **6**, and **7** were again tested under the same conditions mentioned before with the addition of 0.75 mol% of TBAI. All the reactions were carried out under solvent-free conditions.

Author contributions

Conceptualization, D. M. and R. S. R.; investigation, A. A., F. G. Z. and N. K.; X-ray structural studies: S. M-L.; DFT calculations, N. V.-E.; writing – original draft preparation, A. A., F. G. Z., R. S. R., E. M. and D. M.; writing – review and editing, A. A., F. G. Z., R. S. R. E. M. and D. M.; supervision, E. M., R. S. R and D. M.; project administration, R. S. R. and D. M.; and funding acquisition, D. M. and R. S. R. All authors have read and agreed to the published version of the manuscript.

Conflicts of interest

There are no conflicts to declare.

Data availability

Additional data supporting this article have been included as part of the supplementary information (SI). Supplementary information: additional experimental information, NMR spectra, crystallographic data and DFT calculations. See DOI: https://doi.org/10.1039/d5dt02221e.

CCDC 2477633 and 2477634 contain the supplementary crystallographic data for this paper.[27a,b]

Acknowledgements

This work was supported by the Centre National de la Recherche Scientifique (CNRS), the Université de Toulouse, ECOS–Sud Chili (No. C19E04), and FONDECYT (project no. 1200748; 1230537). A. A. acknowledges funding from Ph.D. ANID 2019 fellowship no. 21190209. F. G. Z. acknowledges funding from Ph.D. ANID 2021 fellowship no. 21210371. N. V. E. acknowledges VRID Iniciación Grant No. 2024001183INI at the Universidad de Concepción and Fondecyt Regular Projects 1220355 and 1221803. This research was supported by the high-performance computing system of PIDi-UTEM (SCC-PIDi-UTEM CONICYT-FONDEQUIP-EQM180180).

References

1 J. Pospech, I. Fleischer, R. Franke, S. Buchholz and M. Beller, *Angew. Chem., Int. Ed.*, 2013, **52**, 2852–2872, DOI: 10.1002/anie.201208330.

2 F. Godoy, C. Segarra, M. Poyatos and E. Peris, *Organometallics*, 2011, **30**, 684–688, DOI: 10.1021/om100960t.

3 J. Takagi, K. Takahashi, T. Ishiyama and N. Miyaura, *J. Am. Chem. Soc.*, 2002, **124**, 8001–8006, DOI: 10.1021/ja0202255.

4 N. A. Tappe, R. M. Reich, V. D'Elia and F. E. Kühn, *Dalton Trans.*, 2018, **47**, 13281–13313, DOI: 10.1039/C8DT02346H.

5 Q. Liu, L. Wu, R. Jackstell and M. Beller, *Nat. Commun.*, 2015, **6**, 5933, DOI: 10.1038/ncomms6933.

6 J. Yun, L. Zhang, Q. Qu, H. Liu, X. Zhang, M. Shen and H. Zheng, *Electrochim. Acta*, 2015, **167**, 151–159, DOI: 10.1016/j.electacta.2015.03.159.

7 J. H. Clements, *Ind. Eng. Chem. Res.*, 2003, **42**, 663–674, DOI: 10.1021/ie020678i.

8 P. P. Pescarmona, *Curr. Opin. Green Sustainable Chem.*, 2021, **29**, 100457, DOI: 10.1016/j.cogsc.2021.100457.

9 *Handbook of Aluminum: Volume 2: Alloy Production and Materials Manufacturing*, ed. G. E. Totten and D. S. MacKenzie, New York, Basel, 2003.

10 K. Hobson, C. J. Carmalt and C. Bakewell, *Chem. Sci.*, 2020, **11**, 6942–6956, DOI: 10.1039/D0SC02686G.

11 (*a*) M. P. Coles, D. C. Swenson and R. F. Jordan, *Organometallics*, 1997, **16**, 5183–5194, DOI: 10.1021/om9706323; (*b*) M. P. Coles and R. F. Jordan, *J. Am. Chem. Soc.*, 1997, **119**, 8125–8126, DOI: 10.1021/ja971815j; (*c*) M. P. Coles, D. C. Swenson and R. F. Jordan, *Organometallics*, 1998, **17**, 4042–4048, DOI: 10.1021/om9802358; (*d*) S. Dagorne, I. A. Guzei, M. P. Coles and R. F. Jordan, *J. Am. Chem. Soc.*, 2000, **122**, 274–289, DOI: 10.1021/ja992104j; (*e*) D. Doyle, Y. K. Gun'ko, P. B. Hitchcock and M. F. Lappert, *J. Chem. Soc., Dalton Trans.*, 2000, 4093–4097, DOI: 10.1039/B005824F; (*f*) D. Abeysekera, K. N. Robertson, T. S. Cameron and J. A. C. Clyburne, *Organometallics*, 2001, **20**, 5532–5536, DOI: 10.1021/om010752h; (*g*) H. A. Jenkins, D. Abeysekera, D. A. Dickie and J. A. C. Clyburne, *J. Chem. Soc., Dalton Trans.*, 2002, 3919–3922, DOI: 10.1039/B205875H; (*h*) B. Clare, N. Sarker, R. Shoemaker and J. R. Hagadorn, *Inorg. Chem.*, 2004, **43**, 1159–1166, DOI: 10.1021/ic035035p; (*i*) A. L. Brazeau and S. T. Barry, *Chem. Mater.*, 2008, **20**, 7287–7291, DOI: 10.1021/cm802195b; (*j*) F. Qian, K. Liu and H. Ma, *Dalton Trans.*, 2010, **39**, 8071–8083, DOI: 10.1039/C0DT00272K; (*k*) Y. R. Yepes, J. Martínez, H. R. Sánchez, C. Quintero, M. C. Ortega-Alfaro, J. G. López-Cortés, C. G. Daniliuc, A. Antiñolo, A. Ramos and R. S. Rojas, *Dalton Trans.*, 2020, **49**, 1124–1134, DOI: 10.1039/C9DT03808F; (*l*) K. Hobson, C. J. Carmalt and C. Bakewell, *Inorg. Chem.*, 2021, **60**, 10958–10969; (*m*) S. Banerjee, C. A. Kumar, S. Bose, S. K. Sarkar, S. K. Gupta, N. Graw, C. Köhler, R. Herbst-Irmer, D. Stalke, S. Dutta, D. Koley and H. W. Roesky, *Z. Anorg. Allg. Chem.*, 2021, **647**, 1735–1743; (*n*) C. Ni, X. Ma, Z. Yang and H. W. Roesky, *Eur. J. Inorg. Chem.*, 2022, e202100929, DOI: 10.1002/ejic.202100929; (*o*) F. Gómez Zamorano, M. J. Rojas, S. Mallet-Ladeira, A. R. Cabrera, J. Garo, J.-M. Sotiropoulos, E. Maerten, D. Madec and R. S. Rojas, *Molecules*, 2025, **30**, 3842–3859, DOI: 10.3390/molecules30193842.

12 T. Ishikawa and T. Kumamoto, in *Superbases for Organic Synthesis*, John Wiley & Sons, Ltd, 2009, pp. 49–91, DOI: 10.1002/9780470740859.ch3.

13 A. A. Aly and A. M. Nour-El-Din, *ARKIVOC*, 2008, **1**, 153–194, DOI: 10.3998/ark.5550190.0009.106.

14 D. O. Meléndez, A. Lara-Sánchez, J. Martínez, X. Wu, A. Otero, J. A. Castro-Osma, M. North and R. S. Rojas, *ChemCatChem*, 2018, **10**, 2271–2277, DOI: 10.1002/cctc.201702014.

15 Y. R. Yepes, C. Quintero, D. O. Meléndez, C. G. Daniliuc, J. Martínez and R. S. Rojas, *Organometallics*, 2019, **38**, 469–478, DOI: 10.1021/acs.organomet.8b00795.

16 S. Saltarini, N. Villegas-Escobar, J. Martínez, C. G. Daniliuc, R. A. Matute, L. H. Gade and R. S. Rojas, *Inorg. Chem.*, 2021, **60**, 1172–1182, DOI: 10.1021/acs.inorgchem.0c03290.

17 A. W. Addison, T. N. Rao, J. Reedijk, J. van Rijn and G. C. Verschoor, *J. Chem. Soc., Dalton Trans.*, 1984, 1349–1356, DOI: 10.1039/DT9840001349.

18 L. Yang, D. R. Powell and R. P. Houser, *Dalton Trans.*, 2007, 955–964, DOI: 10.1039/B617136B.

19 N. Villegas-Escobar, D. E. Ortega, D. Cortés-Arriagada, R. Durán, D. Yepes, S. Gutiérrez-Oliva and A. Toro-Labbé, *J. Phys. Chem. C*, 2017, **121**, 12127–12135, DOI: 10.1021/acs.jpcc.7b00278.

20 M. V. Yakovenko, A. V. Cherkasov, G. K. Fukin, D. Cui and A. A. Trifonov, *Eur. J. Inorg. Chem.*, 2010, 3290–3298, DOI: 10.1002/ejic.201000330.

21 A. Acuña, S. Mallet-Ladeira, J.-M. Sotiropoulos, E. Maerten, A. R. Cabrera, A. Baceiredo, T. Kato, R. S. Rojas and D. Madec, *Molecules*, 2024, **29**, 325, DOI: 10.3390/molecules29020325.

22 Bruker, *SADABS*, Bruker AXS Inc., Madison, Wisconsin, USA, 2008.

23 G. M. Sheldrick, *Acta Crystallogr., Sect. A: Found. Adv.*, 2015, **71**, 3–8, DOI: 10.1107/S2053273314026370.

24 G. M. Sheldrick, *Acta Crystallogr., Sect. C: Struct. Chem.*, 2015, **71**, 3–8, DOI: 10.1107/S2053229614024218.

25 A. L. Spek, *Acta Crystallogr., Sect. C: Struct. Chem.*, 2015, **71**, 9, DOI: 10.1107/S2053229614024929.

26 A. J. Bridgeman, G. Cavigliasso, L. R. Ireland and J. Rothery, *Dalton Trans.*, 2001, 2095–2108, DOI: 10.1039/b102094n.

27 (*a*) CCDC 2477633: Experimental Crystal Structure Determination, 2025, DOI: 10.5517/ccdc.csd.cc2p55nq; (*b*) CCDC 2477634: Experimental Crystal Structure Determination, 2025, DOI: 10.5517/ccdc.csd.cc2p55pr.